JOURNAL OF VIROLOGY, May 2001, p. 4802–4813 Vol. 75, No. 10
0022-538X/01/$04.00+0 DOI: 10.1128/JVI.75.10.4802–4813.2001

Visualization of Intracellular Movement of Vaccinia Virus Virions Containing a Green Fluorescent Protein-B5R Membrane Protein Chimera

BRIAN M. WARD AND BERNARD MOSS*

Laboratory of Viral Diseases, National Institute of Allergy and Infectious Diseases, National Institutes of Health, Bethesda, Maryland 20892-0445

Received 1 November 2000/Accepted 16 February 2001

We produced an infectious vaccinia virus that expressed the B5R envelope glycoprotein fused to the enhanced green fluorescent protein (GFP), allowing us to visualize intracellular virus movement in real time. Previous transfection studies indicated that fusion of GFP to the C-terminal cytoplasmic domain of B5R did not interfere with Golgi localization of the viral protein. To determine whether B5R-GFP was fully functional, we started with a B5R deletion mutant that made small plaques and inserted the B5R-GFP gene into the original B5R locus. The recombinant virus made normal-sized plaques and acquired the ability to form actin tails, indicating reversal of the mutant phenotype. Moreover, immunogold electron microscopy revealed that both intracellular enveloped virions (IEV) and extracellular enveloped virions contained B5R-GFP. By confocal microscopy of live infected cells, we visualized individual fluorescent particles, corresponding to IEV in size and shape, moving from a juxtanuclear location to the periphery of the cell, where they usually collected prior to association with actin tails. The fluorescent particles could be seen emanating from cells at the tips of microvilli. Using a digital camera attached to an inverted fluorescence microscope, we acquired images at 1 frame/s. At this resolution, IEV movement appeared saltatory; in some frames there was no net movement, whereas in others movement exceeded 2 μm/s. Further studies indicated that IEV movement was reversibly arrested by the microtubule-depolymerizing drug nocodazole. This result, together with the direction, speed, and saltatory motion of IEV, was consistent with a role for microtubules in intracellular transport of IEV.

Vaccinia virus morphogenesis is a complex process that begins with the formation of crescent membranes within cytoplasmic factory regions and leads to the production of infectious intracellular mature virions (IMV) (6, 13, 19, 38). After IMV are transported away from the factories, some are wrapped with a double membrane derived from the trans-Golgi network (TGN) or endosomal cisternae to form intracellular enveloped virions (IEV) (15, 36, 40). By associating with actin tails (4) or through other mechanisms (41, 44), the IEV reach the periphery of the cell, where one of the two outer membranes is thought to fuse with the plasma membrane. The externalized virions remain attached to the outer surface of the cell as cell-associated extracellular enveloped virions or are released as extracellular enveloped virions (EEV). The cell-associated extracellular enveloped virions and EEV are thought to be responsible for cell-to-cell (2) and long-range (26) virus spread, respectively.

The proteins encoded by the F13L, B5R, A33R, A34R, A36R, and A56R open reading frames (ORFs) are constituents of the IEV or EEV membrane (7, 9, 20, 25, 28, 32, 41). Deletion of any one of these ORFs except A56R, which encodes the viral hemagglutinin, resulted in a mutant virus with a small-plaque phenotype. The F13L and B5R proteins are required for EEV formation, because deletion of either severely reduced the wrapping of IMV to form IEV (1, 10, 43). In contrast, deletion of the A33R, A34R, or A36R gene leads to the absence of actin tails without blocking EEV formation, suggesting that actin tails are more important for cell-to-cell spread than for egress (31, 34, 44, 46).

The trafficking of proteins from the endoplasmic reticulum to the Golgi network and to the plasma membrane has been visualized by transfecting cells with a plasmid that expresses vesicular stomatitis virus envelope glycoprotein (VSVG) fused to enhanced green fluorescent protein (GFP) (17, 30). In a similar manner, we previously demonstrated the localization of a vaccinia virus B5R-GFP fusion protein in Golgi membranes of uninfected cells and identified the targeting signals involved in that process (42). Although the C-terminal attachment of the GFP sequence did not affect the intracellular trafficking of the B5R protein, we did not know whether it would compromise B5R function. Since the B5R protein is required for the formation of IEV, actin tail formation, and virus spread, the most rigorous way of evaluating the functionality of the B5R-GFP fusion would be to substitute the gene encoding the chimeric protein for the natural one. We now describe the construction and characterization of a B5R-GFP recombinant vaccinia virus, the use of confocal and fluorescence video microscopy to visualize the intracellular movement of the IEV, and the effect of a microtubule-depolymerizing drug on this movement.

MATERIALS AND METHODS

Construction of B5R-GFP virus. The construction of a plasmid containing the B5R ORF and approximately 500 bp of flanking sequence on each side (pBMW-4) and another with the B5R ORF fused to GFP sequences (pB5R-

* Corresponding author. Mailing address: 4 Center Dr., MSC 0445, National Institutes of Health, Bethesda, MD 20892-0445. Phone: (301) 496-9869. Fax: (301) 480-1147. E-mail: bmoss@nih.gov.

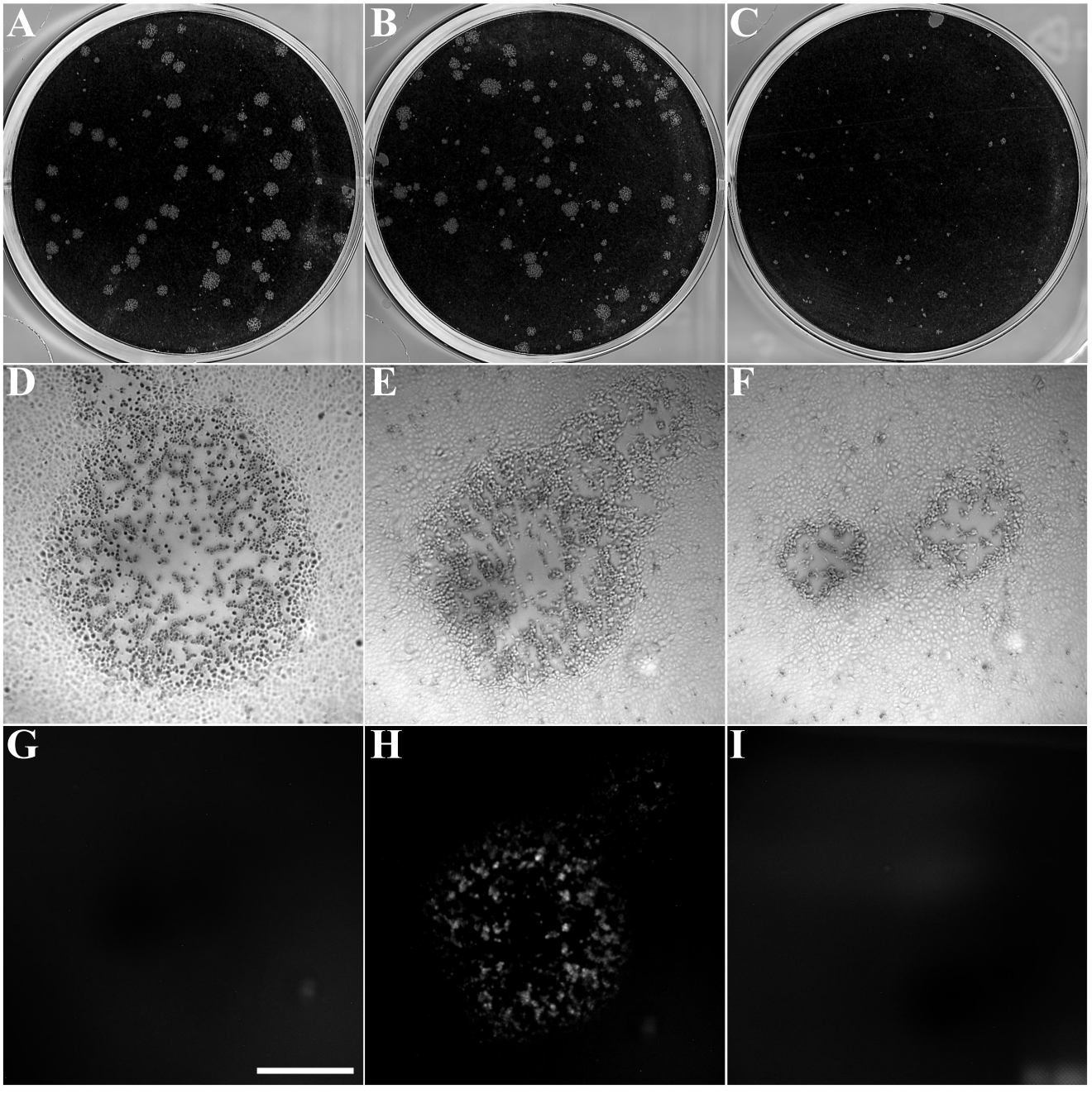

FIG. 1. Plaque phenotype of vB5R-GFP. Viruses were plated on monolayers of BS-C-1 cells. After 2 days, plaques were either stained with crystal violet (top panels) or viewed by differential interference contrast (middle panels) and fluorescence (bottom panels) microscopy. (A, D, and G) Vaccinia virus strain WR; (B, E, and H) vB5R-GFP; (C, F, and I) B5R deletion mutant. Scale bar, 0.5 cm (D through I).

GFP) has been described previously (42). A *Not*I site was introduced using the primers AGCGGCCGCTAAATATAAATCCGTTAAAATAAT and M13 Rev (Promega) with pBMW-4 as the template. The resulting fragment was cloned into pGEM-T and sequenced. To construct a plasmid that contained B5R-GFP and approximately 500 bp of the flanking sequence on each side, a three-fragment ligation was set up using (i) *Hpa*I- and *Nsi*I-digested pBMW-4 as the vector fragment, (ii) the *Hpa*I-*Not*I fragment from pB5R-GFP which contained the last one-third of B5R and GFP, and (iii) the *Not*I-*Nsi*I fragment from the pGEM-T construct described above. The resulting plasmid was transfected with Lipofectamine (GIBCO-BRL) into HeLa cells that had been infected with vaccinia virus vSI-14 (43), in which B5R has been replaced with a *lac*Z-*gpt* cassette. Recombinant viruses that formed green fluorescent foci were plaque purified three times. The final plaques were screened for β-galactosidase synthesis to make sure that the recombinant virus did not retain the *lac*Z-*gpt* cassette. The resulting recombinant virus (called vBMW-1 or vB5R-GFP) was amplified and analyzed by PCR using primers that annealed just upstream and downstream of the B5R ORF. The size of the PCR product was in accordance with insertion of the full B5R-GFP ORF, and the wild-type-sized B5R PCR product was not detected.

Cells and viruses. HeLa and BS-C-1 cell monolayers were grown in Dulbecco's modified Eagle's medium and Earle's minimum essential medium (Quality Biologicals), respectively, supplemented with 10% fetal bovine serum. Virus was propagated in HeLa cells, and plaque assays were carried out with BS-C-1 cells by standard procedures. Images were obtained at 2 days after infection, using a

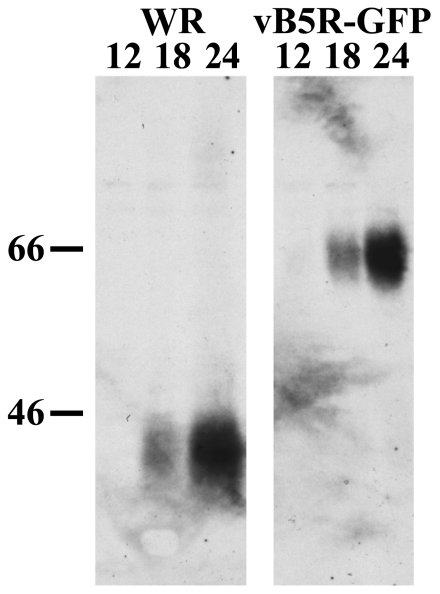

FIG. 2. Synthesis of B5R-GFP. HeLa cells were infected with WR or vB5R-GFP. At various time points, cells were harvested and analyzed by sodium dodecyl sulfate-polyacrylamide gel electrophoresis and Western blotting with MAb 19C2 to B5R. The numbers above the lanes indicate the hour after infection that the cells were harvested. The masses (in kilodaltons) and positions of marker proteins are shown on the left.

Leica DMIRBE inverted fluorescence microscope with a cooled charged-coupled device camera (Princeton Instruments) that was controlled by using Image Pro software.

Western blotting. HeLa cells were infected with 10 PFU of virus per cell. At various time points, cells were scraped from the dish and collected by centrifugation. Pelleted cells were dissolved in lysis buffer (100 mM Tris [pH 8.0], 100 mM NaCl, 0.5% Triton X-100, and 0.2 M phenylmethylsulfonyl fluoride), incubated on ice for 10 min, and stored at −80°C until samples were collected at all time points. Lysed extracts were resolved by sodium dodecyl sulfate–12% polyacrylamide gel electrophoresis and transferred to a nitrocellulose membrane. Membranes were incubated with anti-B5R monoclonal antibody (MAb) 19C2 (36) followed by horseradish peroxidase-conjugated goat anti-rat antibody (Jackson ImmunoResearch Laboratories). Bound antibodies were detected with chemiluminescence reagents (Pierce) as directed by the manufacturer.

Fluorescence microscopy of fixed cells. HeLa cells were grown to confluence on coverslips and infected at a multiplicity of 1. Infected cells were fixed with 4% paraformaldehyde and permeabilized with Triton X-100, both diluted in phosphate-buffered saline. To stain intracellular virions, fixed and permeabilized cells were incubated with anti-B5R MAb 19C2 followed by indodicarbocyanine (Cy5)-conjugated goat anti-rat secondary antibody (Jackson ImmunoResearch Laboratories) that had been diluted 1:100 in phosphate-buffered saline. Actin filaments were stained with rhodamine-conjugated phalloidin (Molecular Probes), and coverslips were mounted in Mowio containing 1 μg of 4′,6-diamidino-2-phenylindole dihydrochloride (DAPI) (Molecular Probes) per ml to visualize DNA in the nucleus and viral factories. Images were collected on a Leica TCS-NT/SP inverted confocal microscope with an attached Argon laser (Coherent Inc.). Images were overlaid by using Adobe PhotoShop version 5.5.

Fluorescence microscopy of live cells. HeLa cells were plated at ~80% confluence onto ΔTC3 dishes (Bioptechs, Inc.) and infected with 0.2 PFU of virus per cell on the next day. On the following day, cells were imaged by either confocal or video microscopy. In some experiments, synchronization of virus assembly was achieved by adding 0.1 mg of rifampin per ml of medium at 1 h after infection and removing it 3 h prior to imaging. A Bio-Rad MicroRadiance confocal scanning system attached to a Zeiss Axiovert 135 microscope was used for confocal microscopy. For video microscopy, a Hammumatsu C5985 camera and controller were attached to a Leica DMIRBE inverted fluorescence microscope. Images were digitized using an IC-PCI video capture card (Coreco Imaging, Inc.) controlled by Image Pro Plus software. In either case, cells were maintained on a heated ΔTC3 stage (Bioptechs) with the temperature set at 35°C. Fresh medium supplemented with 2.5% fetal calf serum and 25 mM HEPES was perfused onto the dish at a rate of 0.1 ml/min throughout the experiment by the use of a P720 peristaltic pump (Instech Laboratories). In some experiments, the perfused medium contained 30 μM nocodazole or 0.1 mg of rifampin/ml for various periods of time. Velocities of virion movement were calculated using the public-domain software NIH Image 1.62 (developed at the National Institutes of Health and available on the internet at http://rsb.info.nih.gov/nih-image/).

Cryoimmunoelectron microscopy. RK_{13} cells were grown in 60-mm-diameter dishes and infected with vaccinia virus at a multiplicity of 10. After 24 h, the cells were prepared for freezing as previously described (45) except that the final fixation step was performed with 8% paraformaldehyde. Ultrathin sections were cut, collected, immunostained, and viewed as previously described (5). The GFP polyclonal antibody (Clontech) was used at a dilution of 1:75.

RESULTS

Construction of a recombinant vaccinia virus that expresses a B5R-GFP fusion protein. Having shown by transfection experiments that the addition of GFP to the C terminus of the vaccinia virus B5R envelope glycoprotein did not affect the normal intracellular targeting of this protein to the Golgi network (42), we wanted to determine whether the chimeric protein could functionally replace wild-type B5R during vaccinia virus infection. To accomplish this, we started with the vaccinia virus mutant vSI-14, in which the B5R gene has been largely replaced with a *lacZ-gpt* cassette (43). HeLa cells were infected with the B5R deletion mutant and transfected with a plasmid containing B5R-GFP and B5R-flanking sequences including the natural B5R promoter. Recombinant virus plaques exhibiting green fluorescence were picked. Individual recombinant viruses were further plaque purified and screened by PCR to confirm the presence of the ORF encoding the B5R fusion protein and the absence of the wild-type B5R ORF (data not shown). In addition to exhibiting fluorescence, the plaques formed by the B5R-GFP virus were considerably larger than those of the parental B5R deletion mutant and resembled plaques formed by WR, suggesting that the fusion protein was functional (Fig. 1).

Expression of B5R-GFP was demonstrated by Western blotting with a MAb to the B5R protein. Cells were infected with either WR or vB5R-GFP and harvested at various time points. In each case, a prominent band was detected at 18 and 24 h (Fig. 2). As expected, the B5R-GFP fusion protein was approximately 20-kDa larger than the wild-type B5R protein, and there was no trace of the latter in cells infected with vB5R-GFP.

FIG. 3. Confocal microscopy of cells infected with vB5R-GFP. HeLa cells were infected with WR (A) or vB5R-GFP (B to F) and then stained with MAb 19C2 against B5R followed by Cy5-conjugated donkey anti-rat antibody (appearing white [A] or red [E and F]). F-actin was visualized with rhodamine-phalloidin (red [A, C, and D]). GFP fluorescence appears green (B, D, and F). (D) Overlay of panels B and C; (F) overlay of panels B and E. Overlapping red and green signal is represented by yellow (D and F). Arrowheads indicate virions on the end of actin tails. Arrowheads in panels B and D to F point to the same set of virions.

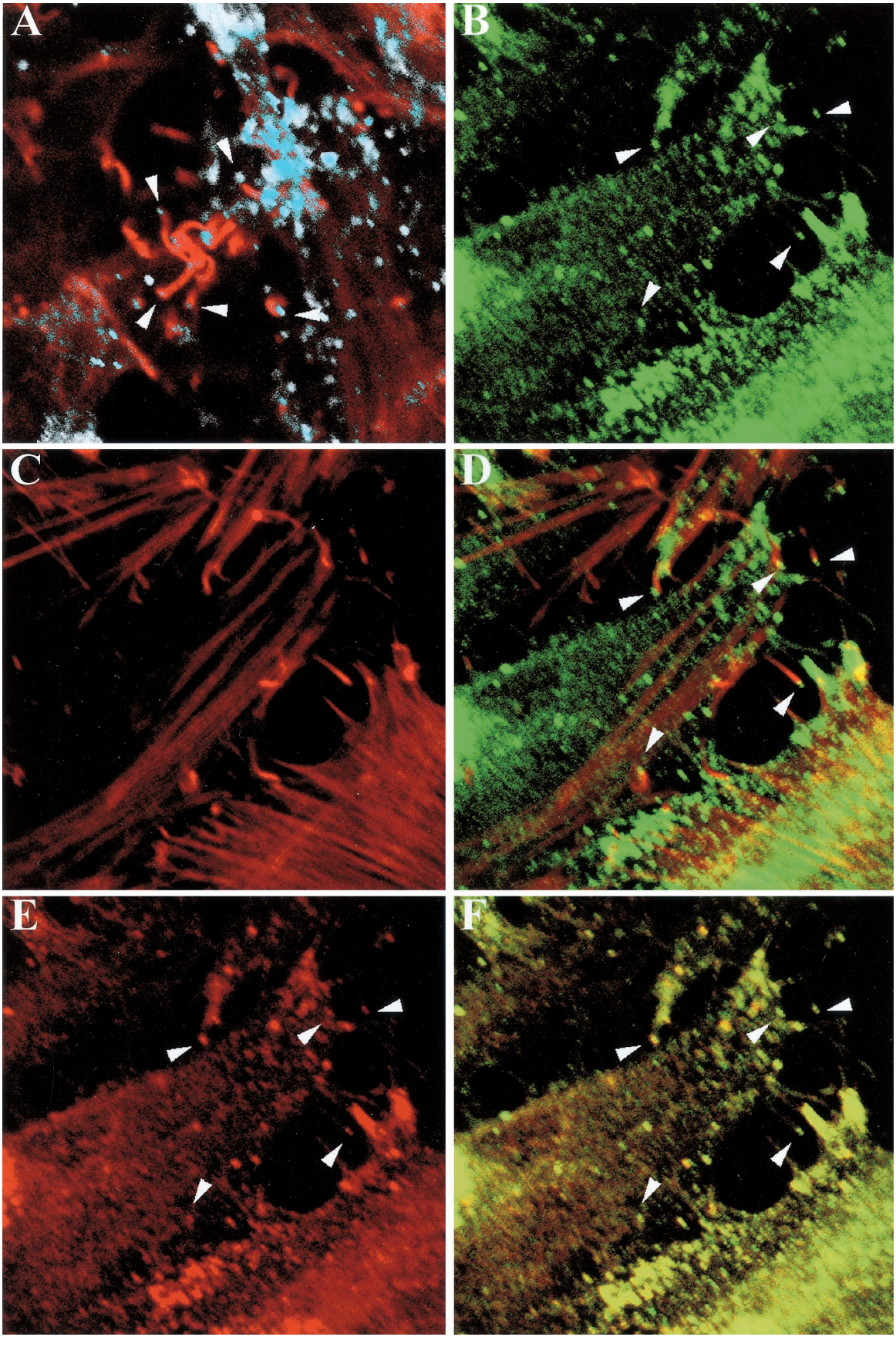
A
B
C
D
E
F

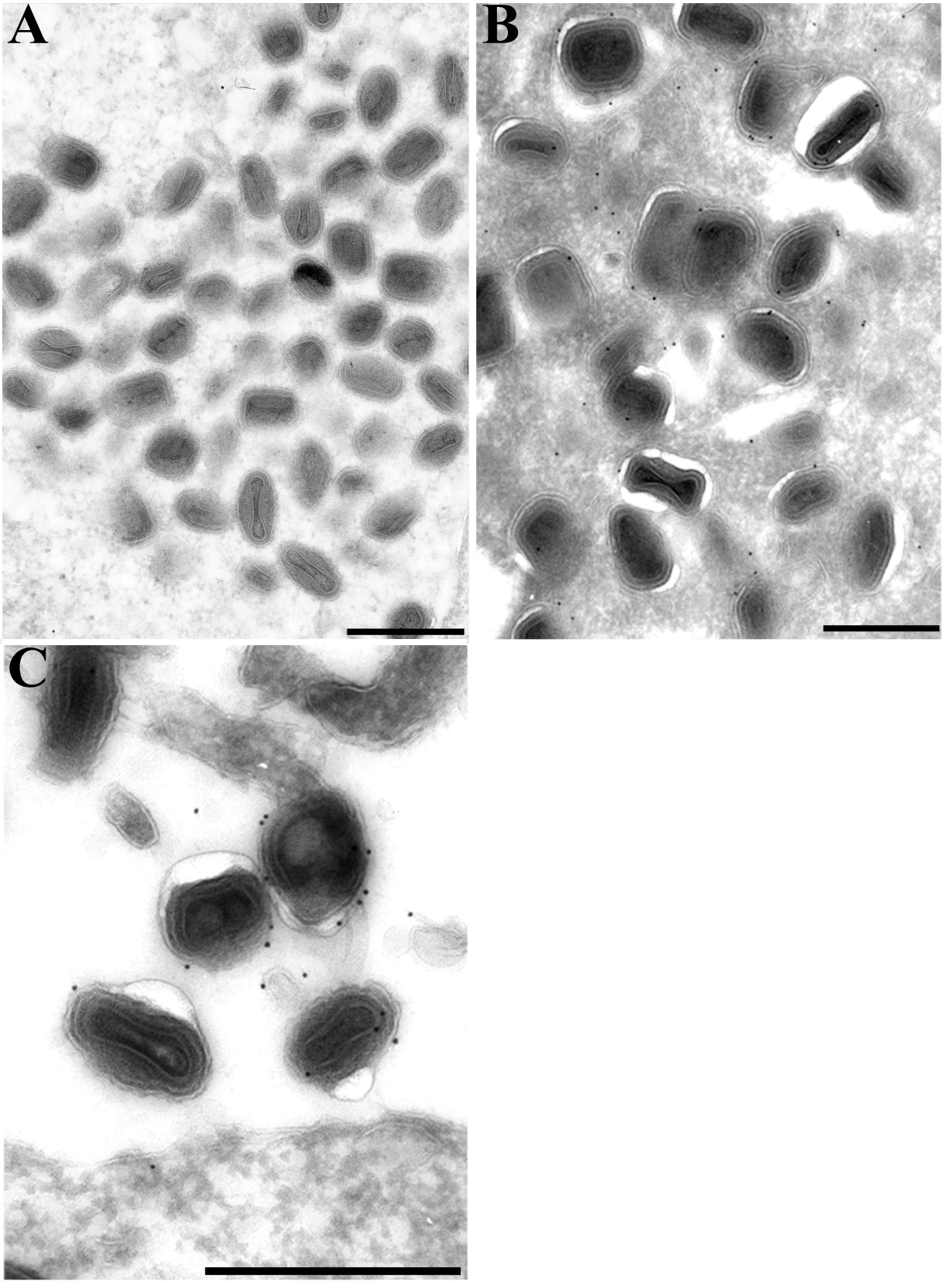

FIG. 4. Immunogold electron microscopy of cells infected with vB5R-GFP. RK_{13} cells that had been infected with vB5R-GFP for 24 h were fixed in paraformaldehyde, cryosectioned, and incubated with GFP polyclonal antibody followed by 10-nm-diameter gold particles conjugated to protein A. IMV (A), IEV (B), and EEV (C) are shown. Scale bars, 500 nm.

TABLE 1. Frame-by-frame measurements for five individual virions

Frame no.[a]	Measurement (μm) for frame:				
	A	B	C	D	E
1	0.98	0.95	0.00	0.81	0.00
2	0.57	0.70	0.00	1.63	2.20
3	0.00	0.00	0.70	0.77	1.06
4	0.00	0.36	1.21	1.07	0.88
5	0.57	0.69	0.98	2.48	1.31
6	0.00	0.00	0.29	2.05	1.09
7	0.00	0.95	0.00	0.00	0.00
8	0.00	1.39	0.93	2.40	1.83
9	0.24	0.75	0.00	0.00	1.50
10	0.33	1.18	0.57	1.01	1.03
11	0.50	0.33	0.00	0.81	0.95
12	0.36	0.69	0.00	0.00	0.34
13	0.00	0.00	1.56	0.00	
14	0.00	0.00	0.70	0.52	
15	0.00	0.00	1.09	1.29	
16	0.55	0.00	0.98	0.99	
17	0.32	0.00	0.34	1.11	
18	0.00	0.74	0.26	0.00	
19	0.00	0.00	1.20	0.93	
20	0.66	0.00	0.41	1.09	
21	0.00	1.15	0.34	1.27	
22	0.00	0.00	0.00	1.03	
23			1.09		
24			1.04		
Total (μm)	5.08	9.88	13.70	21.25	12.18
Time (s)	22	22	24	22	12
Speed (μm/s)	0.23	0.45	0.57	0.97	1.02

[a] Frame rate, 1 frame/s.

Further characterization of the B5R-GFP virus. Numerous virus particles with actin tails were seen in cells infected with wild-type vaccinia virus by staining with rhodamine-phalloidin to label F-actin fibers and with a B5R-specific MAb (Fig. 3A). Because of the defect in wrapping of IMV, actin tails are extremely rare in cells infected with a B5R deletion mutant (33) and were not detected with the vSI-14 parental virus (data not shown). In contrast, abundant actin-tailed virions were visualized by green fluorescence and phalloidin staining of cells infected with vB5R-GFP (Fig. 3B to D). Furthermore, when the B5R-GFP virus-infected cells were stained with a MAb to B5R followed by a Cy5-conjugated secondary antibody, the Cy5 signal colocalized with the green fluorescence, indicating that the B5R-GFP fusion protein remained intact (Fig. 3E and F).

The wrapping of IMV to form IEV was blocked in cells infected with the parental B5R deletion mutant (43). However, the formation of IEV in cells with vB5R-GFP was demonstrated by electron microscopy (Fig. 4B). Furthermore, the outer membranes of the majority of IEV (Fig. 4B) and EEV (Fig. 4C) were stained with anti-GFP antibody followed by protein A-gold. In contrast, IMV were only sparsely labeled (Fig. 4A) with an amount similar to a wild-type vaccinia virus control (data not shown) and consistent with the background, indicating that B5R-GFP was not associated with IMV. Thus, both functional and structural studies established that the addition of GFP to the C terminus of the B5R glycoprotein had no apparent deleterious effects.

Visualization of IEV movement by laser-scanning confocal microscopy. The abundant incorporation of B5R-GFP into IEV membranes indicated that it should be possible to visualize the intracellular movement of virions in real time by laser-scanning confocal microscopy of unfixed cells. HeLa cell monolayers were infected with 0.2 PFU of B5R-GFP virus per cell and incubated overnight. The low multiplicity was used to minimize cytopathic effects and allow good separation of infected cells from each other. In some experiments, virus assembly was synchronized by adding rifampin to reversibly inhibit morphogenesis (13, 24) and images were collected after the drug was removed. Under low magnifications, individual green cells in the monolayer were observed (data not shown). At higher magnifications, we discerned a brightly fluorescent juxtanuclear region that most likely included the TGN (Fig. 5A), known from previous studies to be a site of B5R protein localization. In addition, there were fluorescent particles of the diameter (~400 μm) and regular shape expected for IEV, which are much larger than the 70- to 90-nm-diameter irregular vesicles and tubules that typically bud from the Golgi network. The number of IEV particles increased with time after rifampin was removed, and they accumulated in peripheral regions of the cell (Fig. 5B). Many of these fluorescent particles appeared to have exited the cell, but thread-like connections could be seen with transmitted light (shown below). By capturing successive images at intervals of 10 s, we could follow the movement of those individual fluorescent particles that remained within the focal plane. Selected images, with the arrowhead pointing to one fluorescent particle as it moved away from the TGN toward the periphery, are shown in Fig. 5A. Movement of another virus particle in the same cell, but later after rifampin removal and at a higher magnification, is shown with arrowheads in Fig. 5B. The movement of these and numerous other particles can be seen in movies available at http://www.niaid.nih.gov/dir/labs/lvd/moss.htm. As a control, we also imaged infected cells from which rifampin was not removed. No movement of particles that were the size and shape of IEV was observed (Fig. 6).

Images of cells infected in the absence of rifampin are shown in Fig. 5C and D. The discrete TGN was largely disrupted by this time, but numerous IEV were still moving to the periphery. We calculated a velocity for virion movement from the pixel dimensions and the time interval (6 s) between images. Intracellular virion speeds ranged from 0.14 to 0.99 μm/s, with a range of 0.18 to 0.48 μm/s in a single cell. The average speed was 0.34 μm/s (standard deviation, 0.12 μm/s). In addition to these uniformly sized virus particles, long tubular-vesicular structures that often stretched as they moved were observed (Fig. 5D). These tubules resembled post-Golgi structures labeled with VSVG-GFP that were described by Hirschberg et al. (17).

The IEV usually congregated at the periphery of the cell in clusters that increased in size and fluorescence as the infection proceeded. Such clusters of IEV are often seen by electron microscopy (Fig. 4B). Large numbers of virus-tipped microvilli formed at the plasma membrane adjacent to these IEV clusters. Nevertheless, some IEV that transited from within the cytoplasm all the way to the edge of the cell were imaged. White arrowheads in successive frames of Fig. 7 depict one such particle. Upon reaching the plasma membrane, the virion

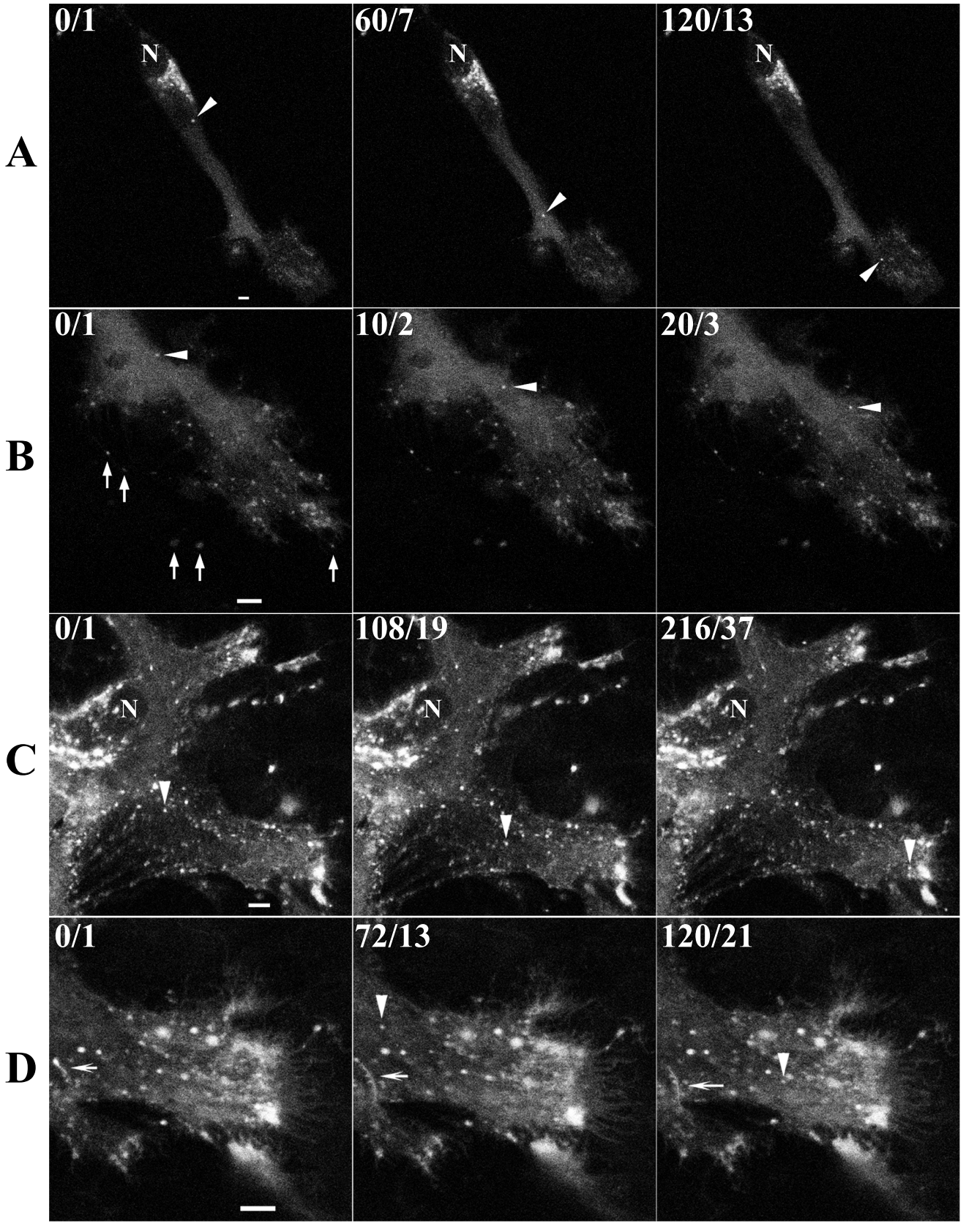
A
0/1
N
60/7
N
120/13
N
B
0/1
10/2
20/3
C
0/1
N
108/19
N
216/37
N
D
0/1
72/13
120/21

appeared at the end of a thread-like projection (Fig. 7, frames 210, 232, 234, and 246). Actin tails could be visualized in the simultaneously captured transmitted light images because of the increased depth of focus. The actin tail attached to the particle being followed was first seen when the particle reached the edge of the cell (Fig. 7, black arrowheads in frames 216, 228, 240, and 252). Additional actin tails, apparently projecting from the cell surface, were also seen in the transmitted-light images (Fig. 7, black arrows).

IEV display saltatory movement. The fastest that we could acquire images with the confocal microscope setup was 1 frame/6 s. With a digital camera attached to an inverted fluorescence microscope, we were able to acquire images at 1 frame/s. With the shorter intervals of time, we discerned that intracellular movement to the cell periphery was composed of frequent stops and starts. Table 1 lists the movement distances, in micrometers per 1-s frame, of five individual virions. In some frames the virions moved quite rapidly (>2 μm), whereas there was no net movement in others. Over the times measured, the average speed of different IEV ranged from 0.23 to 1.02 μm/s.

IEV movement is blocked by nocodazole. The saltatory movement of multiple IEV along similar pathways leading to their accumulation in clusters near the cell periphery suggested the possibility of microtubular transport. To test this hypothesis, cells infected with vB5R-GFP were treated with nocodazole, a drug that disrupts microtubules (18, 22). After imaging a cell displaying normal IEV movement (Fig. 8A), we replaced the medium with medium containing 30 μM nocodazole. After 10 min the number of moving IEV had diminished, and after 50 min there was no discernible movement (Fig. 8B). Only 6 min after the cells were washed with nocodazole-free medium, a particle was seen starting to move toward the cell edge, where it subsequently moved away on a microvillus (Fig. 8C). Subsequently, many particles were seen moving to the plasma membrane and associating with actin tails (Fig. 8D). These results were consistent with a role for microtubules in virion transport.

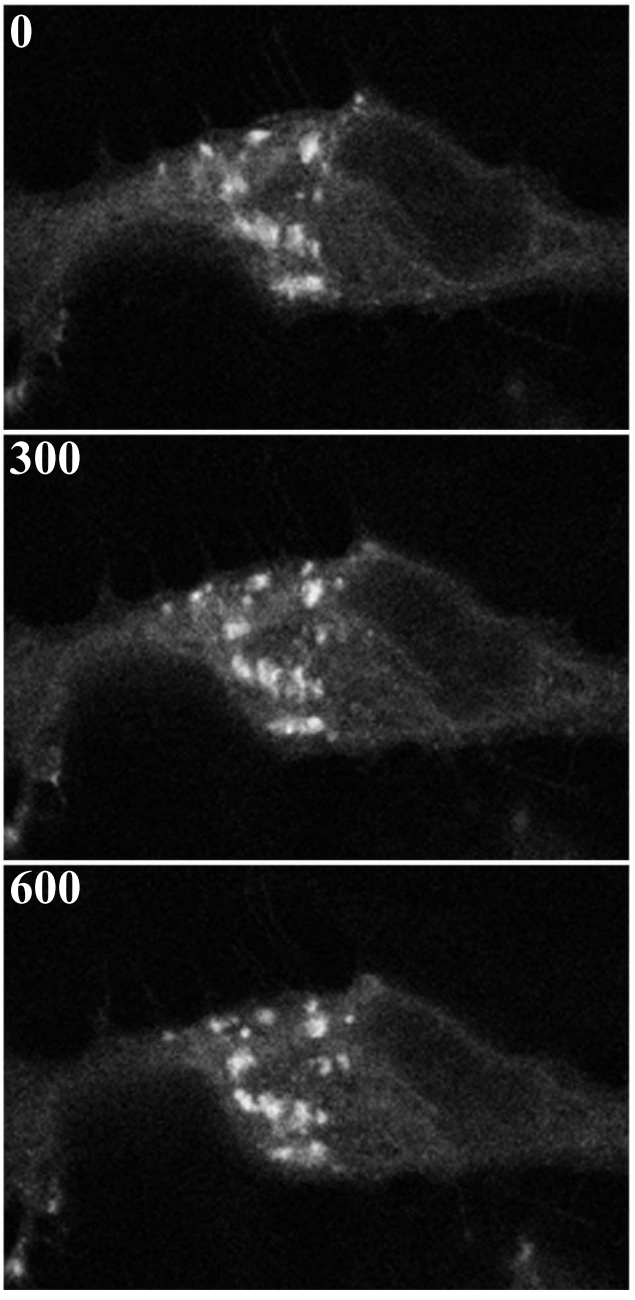

FIG. 6. Effect of rifampin on virion movement. HeLa cells were incubated continuously in medium containing 0.1 μg of rifampin/ml starting 1 h prior to infection with vB5R-GFP. Cells were imaged by confocal microscopy at ~13 h after infection. Shown is a representative cell starting at time zero. Subsequent frames are shown with the cumulative time elapsed (in seconds) indicated in the upper left corner.

DISCUSSION

The poxviruses are among the largest of all animal viruses and have previously been seen by confocal microscopy of fixed and permeabilized cells that were stained with fluorescent antibodies or by phase-contrast video microscopy of unstained, live cells (4). The adaptation of the *Aequorea victoria* GFP for visualizing gene expression and protein localization in living organisms has provided a powerful new tool (3). A study by Elliott and O'Hare (8) showed that the herpes simplex virus P22 tegument protein could be fused to GFP without apparent loss of function. To apply this approach to vaccinia virus, we needed to find a viral structural protein that would retain

FIG. 5. Visualization of IEV by time-lapse confocal microscopy. At 1 h after infection of HeLa cells with 0.2 PFU of vB5R-GFP per cell, medium containing rifampin (0.1 μg/ml) was added to the cell monolayer. Approximately 12 h later, the rifampin was removed by washing with fresh medium. (A) Cells were viewed by confocal microscopy 2 h and 40 min later, and an image of one cell was collected every 10 s for 2 min. (B) After an additional 2 h, an image of the same cell was collected every 10 s. (C and D) HeLa cells were infected with 0.2 PFU of vB5R-GFP in the absence of rifampin, and imaging at 1 frame/6 s was started approximately 12 h later. In the upper left corner, the cumulative time elapsed (in seconds) after the start of image collection/video frame number is indicated. Arrowheads in each row point to the same IEV particle. In row B, the arrows point to virions extended from the cell on microvilli. In row D, the arrows point to tubules. N, nucleus. Scale bars, 50 μm. (The entire time-lapse videos are available at http://www.niaid.nih.gov/dir/labs/lvd/moss.htm.)

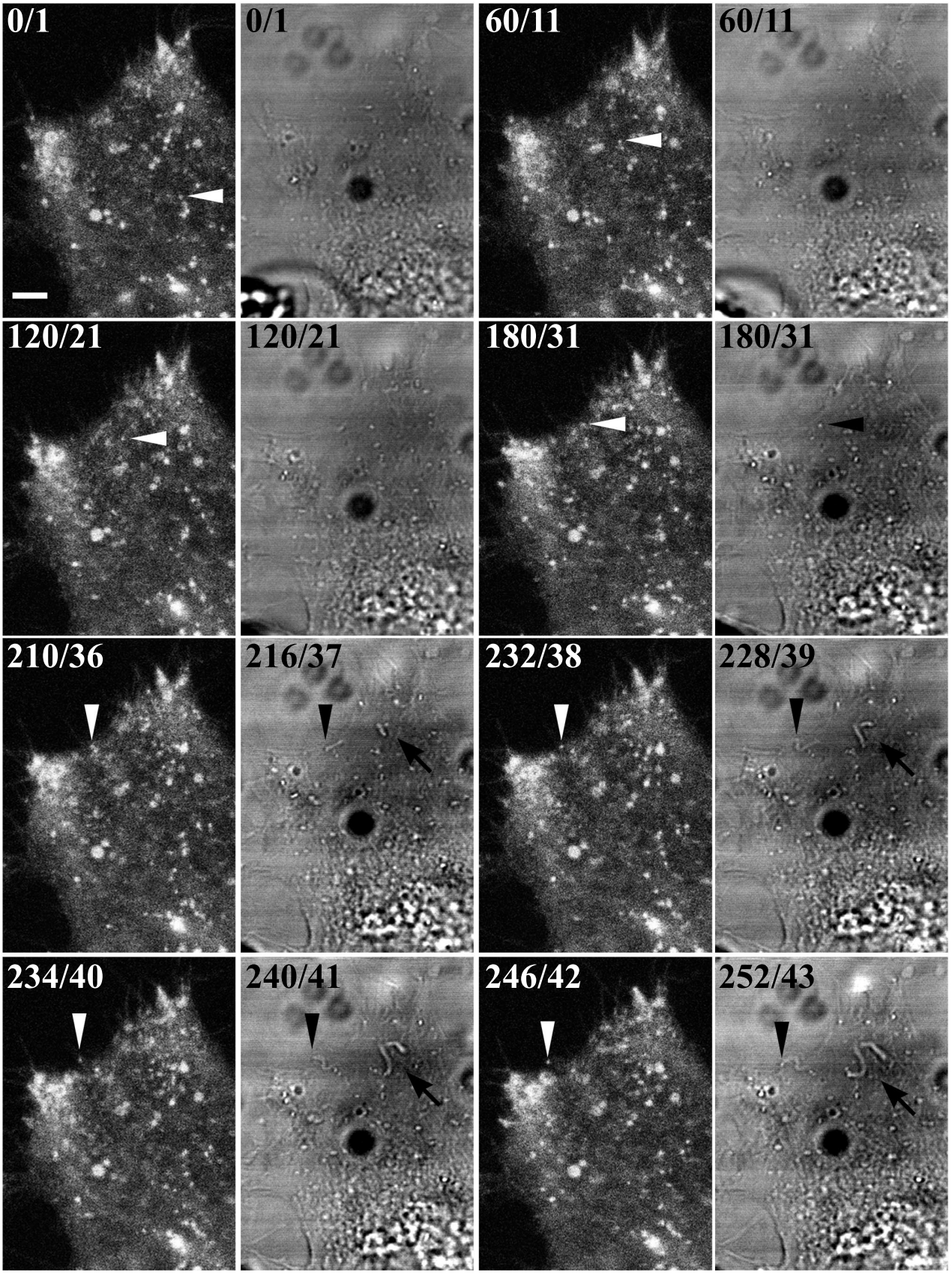

FIG. 7. Visualization of IEV acquiring an actin tail. HeLa cells were infected and examined by confocal microscopy as described in the legend to Fig. 5. One image was acquired every 6 s. As in Fig. 5, the cumulative time elapsed/video frame number of the sequence is indicated in the upper left corner of each image, starting at time/frame 0/1. The frames in the first and third columns depict GFP fluorescence; the frames in the second and fourth columns depict images acquired simultaneously by the transmitted-light detector. Arrowheads point to the same virion in all frames. Arrows point to additional actin tails. Scale bar, 50 μm. (The entire time-lapse videos are available at http://www.niaid.nih.gov/dir/labs/lvd/moss.htm.)

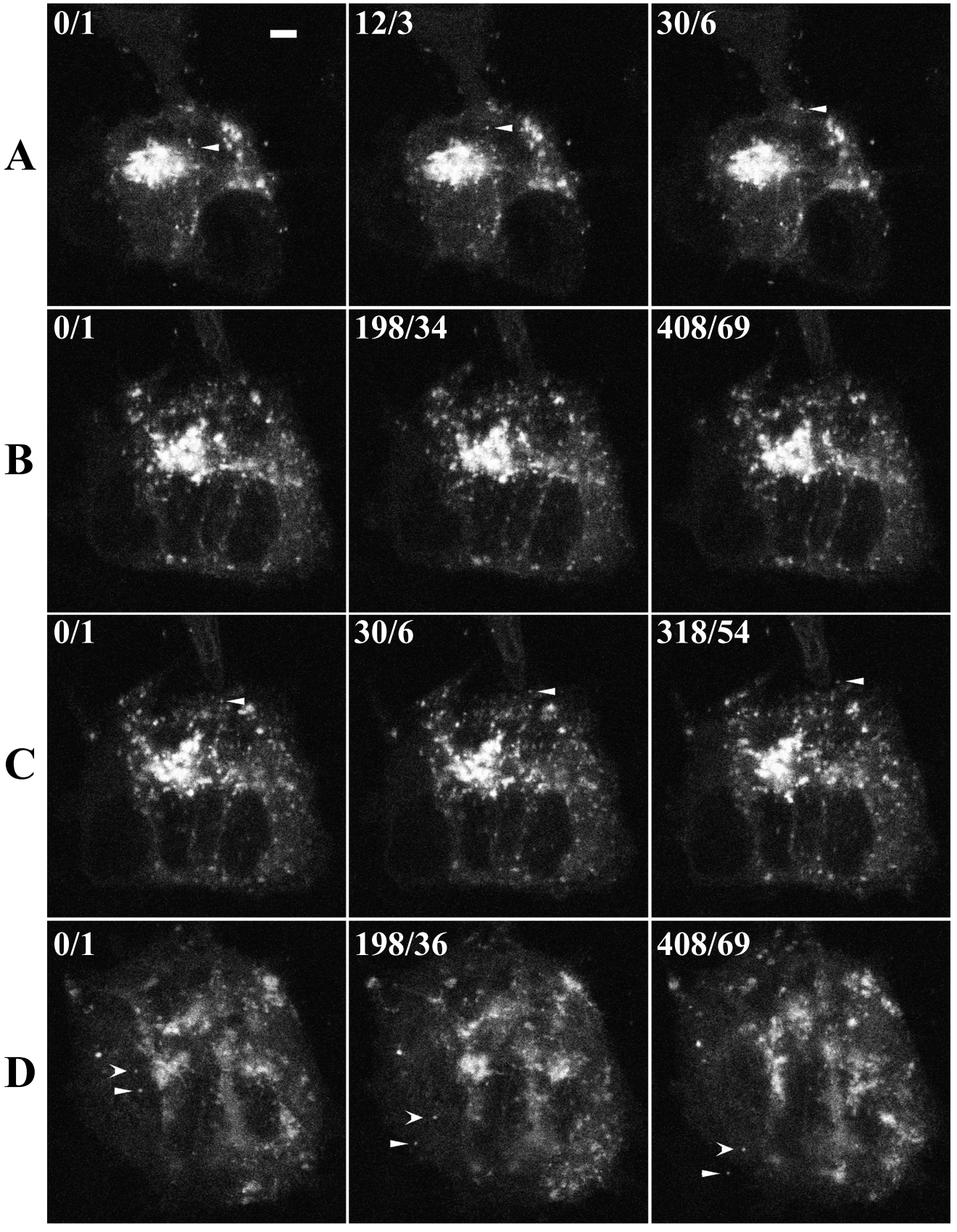

FIG. 8. Effect of nocodazole on virion movement. HeLa cells were infected with vB5R-GFP and examined by confocal microscopy as described in the legend to Fig. 5. One image was acquired every 6 s. (A) No nocodazole added; (B) 50 min after addition of 30 μM nocodazole; (C) 6 min after removal of nocodazole; (D) 97 min after removal of nocodazole. As in Fig. 5, the cumulative time elapsed/video frame number from the sequence is indicated in the upper left corner of each image, starting at time/frame 0/1. Arrowheads point to the same virions in each row. Scale bar, 50 μm. (The entire time-lapse videos are available at http://www.niaid.nih.gov/dir/labs/lvd/moss.htm.)

function when fused to GFP. The EEV-specific type 1 membrane glycoprotein encoded by the B5R gene seemed suitable for several reasons. First, a fusion protein containing the B5R cytoplasmic and transmembrane domains fused to the ectodomain of the human immunodeficiency virus type 1 envelope protein was incorporated into EEV membranes (21). Second, most of the ectodomain of the B5R protein could be deleted without interfering with EEV formation (14, 23). Third, we had shown by transfection experiments that fusion of GFP to the cytoplasmic domain of the B5R protein did not prevent the localization of this protein in the Golgi network (42). We therefore decided to construct a recombinant vaccinia virus in which the B5R-GFP ORF replaced the wild-type B5R ORF. This isolation procedure was facilitated by starting with a vaccinia virus whose B5R gene had been deleted, resulting in a small-plaque phenotype, and using GFP expression as a marker. We found that the recombinant virus formed large, fluorescent plaques, suggesting that the B5R-GFP was functional. This was confirmed by immunoelectron microscopy showing that the B5R-GFP was incorporated into IEV and EEV membranes.

Encouraged by the these results, we examined, by confocal or fluorescence video microscopy, live cells that had been infected with vB5R-GFP. Juxtanuclear structures corresponding to the Golgi network as well as particles of the size and shape expected for IEV were brightly fluorescent. At relatively low illumination levels that did not cause photobleaching or toxicity, we were able to trace the movement of fluorescent particles from a juxtanuclear location to the periphery of the cell and subsequently to microvilli. These B5R-GFP-containing particles were larger and more regular in shape than the elastic post-Golgi transport tubules (17) which were also labeled with B5R-GFP. Furthermore, when vaccinia virus assembly was specifically blocked with the drug rifampin, similar particle movement was not observed. These observations, together with the immunoelectron microscopy data, provided compelling evidence that the fluorescent particles were IEV.

Confocal microscopic images were collected every 6 s to determine the speed of IEV movement from the TGN to the periphery of the cell. The rate of movement was quite variable, but an average value of 0.34 μm/s was determined. This speed was more than 600 times that of the hypothetical diffusion rate of IEV in the cytoplasm that was calculated by Sodeik (37). With a digital camera that was attached to an inverted fluorescence microscope, we were able to acquire images at 1 frame/s. At this resolution, movement was saltatory; in some frames there was no net movement, whereas in others it exceeded 2 μm/s. Saltatory movement and maximal speeds of 2.7 μm/s were also obtained for post-Golgi transport of the smaller VSVG-GFP fusion protein vesicles (16). The saltatory movement of multiple IEV along tracks leading to their accumulation near the cell periphery suggested microtubule involvement, since microtubules are arranged parallel to the long axis of the cell, especially after vaccinia virus infection (29). In addition, the average velocity of the IEV was close to the speed of several classes of kinesin motors that associate with microtubules. The movement of vesicular post-Golgi structures labeled with the VSVG-GFP fusion protein was inhibited by nocodazole, a microtubule-depolymerizing drug (16). Similarly, we found that nocodazole stopped the movement of IEV. A direct effect of nocodazole on IEV movement was suggested because fluorescent particles in the cytoplasm started moving again within minutes after removal of the drug by perfusion of fresh medium. However, nocodazole also interferes with IMV movement and IEV formation (29, 35); hence, further investigation is needed.

Although microtubules and actin filaments had been considered as separate systems, there is growing evidence of physical and functional interactions between them in vesicle and organelle transport (12). Thus, our data supporting a role for microtubules in the long-range intracellular transport of IEV does not preclude a role for cytoskeletal actin filaments in that process. Indeed, we found that cytochalasin D inhibited IEV movement (B. Ward, unpublished data). Several previous studies indicated a role for actin in the release of vaccinia virus from infected cells (4, 27, 39). It has been suggested that actin tails, in contrast to cytoskeletal actin filaments, propel IEV through the cytoplasm to the cell membrane, where long virus-tipped microvilli form (4). However, it is difficult to distinguish particles within the cytoplasm from those at the lower or upper cell surface. Our images suggested that the actin tails first appeared when the IEV were at or near the plasma membrane. A peripheral location for actin tails was also suggested from an analysis of Z sections by confocal microscopy (E. Wolffe, personal communication). Actin tail formation is dependent on three IEV or EEV proteins: A33R, A34R, and A36R (11, 31, 34, 44, 46). When the gene encoding any of these proteins was deleted, virus spread was severely reduced but EEV still formed, indicating that actin tails are not essential for movement of virions to the cell surface. Furthermore, van Eijl et al. (41) presented evidence that the A36R protein is associated with IEV but not EEV and suggested that actin tails form after fusion of the outer IEV membrane with the cell membrane. Thus, microtubules may play a major role in intracellular transport of virions, and the actin tails may facilitate cell-to-cell spread.

ACKNOWLEDGMENTS

We thank members of the Laboratory of Viral Diseases, including Elizabeth Wolffe and Jonathan Yewdell, for advice and help with imaging; Andrea Weisberg for performing the cryoimmunoelectron microscopy; and Norman Cooper for tissue culture cells. Some of the work was carried out in the NIAID imaging facility with the guidance of Owen Schwartz.

REFERENCES

1. **Blasco, R., and B. Moss.** 1991. Extracellular vaccinia virus formation and cell-to-cell virus transmission are prevented by deletion of the gene encoding the 37,000-dalton outer envelope protein. J. Virol. **65:**5910–5920.
2. **Blasco, R., and B. Moss.** 1992. Role of cell-associated enveloped vaccinia virus in cell-to-cell spread. J. Virol. **66:**4170–4179.
3. **Chalfie, M., Y. Tu, G. Euskirchen, W. W. Ward, and D. C. Prasher.** 1994. Green fluorescent protein as a marker for gene expression. Science **263:**802–805.
4. **Cudmore, S., P. Cossart, G. Griffiths, and M. Way.** 1995. Actin-based motility of vaccinia virus. Nature **378:**636–638.
5. **da Fonseca, F. G., E. J. Wolffe, A. Weisberg, and B. Moss.** 2000. Characterization of the vaccinia virus H3L envelope protein: topology and posttranslational membrane insertion via the C-terminal hydrophobic tail. J. Virol. **74:**7508–7517.
6. **Dales, S., and L. Siminovitch.** 1961. The development of vaccinia virus in Earle's L strain cells as examined by electron microscopy. J. Biophys. Biochem. Cytol. **10:**475–503.
7. **Duncan, S. A., and G. L. Smith.** 1992. Identification and characterization of an extracellular envelope glycoprotein affecting vaccinia virus egress. J. Virol. **66:**1610–1621.

8. **Elliott, G., and P. O'Hare.** 1999. Live-cell analysis of a green fluorescent protein-tagged herpes simplex virus infection. J. Virol. **73:**4110–4119.
9. **Engelstad, M., S. T. Howard, and G. L. Smith.** 1992. A constitutively expressed vaccinia gene encodes a 42-kDa glycoprotein related to complement control factors that forms part of the extracellular virus envelope. Virology **188:**801–810.
10. **Engelstad, M., and G. L. Smith.** 1993. The vaccinia virus 42-kDa envelope protein is required for the envelopment and egress of extracellular virus and for virus virulence. Virology **194:**627–637.
11. **Frischknecht, F., V. Moreau, S. Rottger, S. Gonfloni, I. Reckmann, G. Superti-Furga, and M. Way.** 1999. Actin-based motility of vaccinia virus mimics receptor tyrosine kinase signalling. Nature **401:**926–929.
12. **Goode, B. L., D. G. Drubin, and G. Barnes.** 2000. Functional cooperation between the microtubule and actin cytoskeletons. Curr. Opin. Cell Biol. **12:**63–71.
13. **Grimley, P. M., E. N. Rosenblum, S. J. Mims, and B. Moss.** 1970. Interruption by rifampin of an early stage in vaccinia virus morphogenesis: accumulation of membranes which are precursors of virus envelopes. J. Virol. **6:**519–533.
14. **Herrera, E., M. del Mar Lorenzo, R. Blasco, and S. N. Isaacs.** 1998. Functional analysis of vaccinia virus B5R protein: essential role in virus envelopment is independent of a large portion of the extracellular domain. J. Virol. **72:**294–302.
15. **Hiller, G., and K. Weber.** 1985. Golgi-derived membranes that contain an acylated viral polypeptide are used for vaccinia virus envelopment. J. Virol. **55:**651–659.
16. **Hirschberg, K., and J. Lippincott-Schwartz.** 1999. Secretory pathway kinetics and in vivo analysis of protein traffic from the Golgi complex to the cell surface. FASEB J. **13**(Suppl. 2)**:**S251–S256.
17. **Hirschberg, K., C. M. Miller, J. Ellenberg, J. F. Presley, E. D. Siggia, R. D. Phair, and J. Lippincott-Schwartz.** 1998. Kinetic analysis of secretory protein traffic and characterization of Golgi to plasma membrane transport intermediates in living cells. J. Cell Biol. **143:**1485–1503.
18. **Hoebeke, J., G. Van Nijen, and M. De Brabander.** 1976. Interaction of oncodazole (R 17934), a new antitumoral drug, with rat brain tubulin. Biochem. Biophys. Res. Commun. **69:**319–324.
19. **Hollinshead, M., A. Vanderplasschen, G. L. Smith, and D. J. Vaux.** 1999. Vaccinia virus intracellular mature virions contain only one lipid membrane. J. Virol. **73:**1503–1517.
20. **Isaacs, S. N., E. J. Wolffe, L. G. Payne, and B. Moss.** 1992. Characterization of a vaccinia virus-encoded 42-kilodalton class I membrane glycoprotein component of the extracellular virus envelope. J. Virol. **66:**7217–7224.
21. **Katz, E., E. J. Wolffe, and B. Moss.** 1997. The cytoplasmic and transmembrane domains of the vaccinia virus B5R protein target a chimeric human immunodeficiency virus type 1 glycoprotein to the outer envelope of nascent vaccinia virions. J. Virol. **71:**3178–3187.
22. **Liao, G., T. Nagasaki, and G. G. Gundersen.** 1995. Low concentrations of nocodazole interfere with fibroblast locomotion without significantly affecting microtubule level: implications for the role of dynamic microtubules in cell locomotion. J. Cell Sci. **108:**3473–3483.
23. **Mathew, E., C. M. Sanderson, M. Hollinshead, and G. L. Smith.** 1998. The extracellular domain of vaccinia virus protein B5R affects plaque phenotype, extracellular enveloped virus release, and intracellular actin tail formation. J. Virol. **72:**2429–2438.
24. **Moss, B., E. N. Rosenblum, E. Katz, and P. M. Grimley.** 1969. Rifampicin: a specific inhibitor of vaccinia virus assembly. Nature **224:**1280–1284.
25. **Parkinson, J. E., and G. L. Smith.** 1994. Vaccinia virus gene A36R encodes a M_r 43 to 50 K protein on the surface of extracellular enveloped virus. Virology **204:**376–390.
26. **Payne, L. G.** 1980. Significance of extracellular virus in the in vitro and in vivo dissemination of vaccinia virus. J. Gen. Virol. **50:**89–100.
27. **Payne, L. G., and K. Kristensson.** 1982. The effect of cytochalasin D and monensin on enveloped vaccinia virus release. Arch. Virol. **74:**11–20.
28. **Payne, L. G., and E. Norrby.** 1976. Presence of hemagglutinin in the envelope of extracellular vaccinia virus particles. J. Gen. Virol. **32:**63–72.
29. **Ploubidou, A., V. Moreau, K. Ashman, I. Reckmann, C. Gonzalez, and M. Way.** 2000. Vaccinia virus infection disrupts microtubule organization and centrosome function. EMBO J. **19:**3932–3944.
30. **Presley, J. F., N. B. Cole, T. A. Schrer, K. Hirschberg, K. J. M. Zaal, and J. Lippincott-Schwartz.** 1997. ER-to-Golgi transport visualized in living cells. Nature **389:**81–85.
31. **Roper, R. L., E. J. Wolffe, A. Weisberg, and B. Moss.** 1998. The envelope protein encoded by the A33R gene is required for formation of actin-containing microvilli and efficient cell-to-cell spread of vaccinia virus. J. Virol. **72:**4192–4204.
32. **Roper, R. L., L. G. Payne, and B. Moss.** 1996. Extracellular vaccinia virus envelope glycoprotein encoded by the A33R gene. J. Virol. **70:**3753–3762.
33. **Röttger, S., F. Frischknecht, I. Reckmann, G. L. Smith, and M. Way.** 1999. Interactions between vaccinia virus IEV membrane proteins and their roles in IEV assembly and actin tail formation. J. Virol. **73:**2863–2875.
34. **Sanderson, C. M., F. Frischknecht, M. Way, M. Hollinshead, and G. L. Smith.** 1998. Roles of vaccinia virus EEV-specific proteins in intracellular actin tail formation and low pH-induced cell-cell fusion. J. Gen. Virol. **79:**1415–1425.
35. **Sanderson, C. M., M. Hollinshead, and G. L. Smith.** 2000. The vaccinia virus A27L protein is needed for the microtubule-dependent transport of intracellular mature virus particles. J. Gen. Virol. **81:**47–58.
36. **Schmelz, M., B. Sodeik, M. Ericsson, E. J. Wolffe, H. Shida, G. Hiller, and G. Griffiths.** 1994. Assembly of vaccinia virus: the second wrapping cisterna is derived from the trans Golgi network. J. Virol. **68:**130–147.
37. **Sodeik, B.** 2000. Mechanisms of viral transport in the cytoplasm. Trends Microbiol. **8:**465–472.
38. **Sodeik, B., R. W. Doms, M. Ericsson, G. Hiller, C. E. Machamer, W. van't Hof, G. van Meer, B. Moss, and G. Griffiths.** 1993. Assembly of vaccinia virus: role of the intermediate compartment between the endoplasmic reticulum and the Golgi stacks. J. Cell Biol. **121:**521–541.
39. **Stokes, G. V.** 1976. High-voltage electron microscope study of the release of vaccinia virus from whole cells. J. Virol. **18:**636–643.
40. **Tooze, J., M. Hollinshead, B. Reis, K. Radsak, and H. Kern.** 1993. Progeny vaccinia and human cytomegalovirus particles utilize early endosomal cisternae for their envelopes. Eur. J. Cell Biol. **60:**163–178.
41. **van Eijl, H., M. Hollinshead, and G. L. Smith.** 2000. The vaccinia virus A36R protein is a type Ib membrane protein present on intracellular but not extracellular enveloped virus particles. Virology **271:**26–36.
42. **Ward, B. M., and B. Moss.** 2000. Golgi network targeting and plasma membrane internalization signals in vaccinia virus B5R envelope protein. J. Virol. **74:**3771–3780.
43. **Wolffe, E. J., S. N. Isaacs, and B. Moss.** 1993. Deletion of the vaccinia virus B5R gene encoding a 42-kilodalton membrane glycoprotein inhibits extracellular virus envelope formation and dissemination. J. Virol. **67:**4732–4741.
44. **Wolffe, E. J., E. Katz, A. Weisberg, and B. Moss.** 1997. The A34R glycoprotein gene is required for induction of specialized actin-containing microvilli and efficient cell-to-cell transmission of vaccinia virus. J. Virol. **71:**3904–3915.
45. **Wolffe, E. J., S. Vijaya, and B. Moss.** 1995. A myristylated membrane protein encoded by the vaccinia virus L1R open reading frame is the target of potent neutralizing monoclonal antibodies. Virology **211:**53–63.
46. **Wolffe, E. J., A. S. Weisberg, and B. Moss.** 1998. Role for the vaccinia virus A36R outer envelope protein in the formation of virus-tipped actin-containing microvilli and cell-to-cell virus spread. Virology **244:**20–26.